Fuel 325 (2022) 124813

Contents lists available at ScienceDirect

Fuel

journal homepage: www.elsevier.com/locate/fuel

Full length article

Holographic slurry droplet monitor: Design and its application to 1000 MW coal-fired power unit

Zhiming Lin [a], Yingchun Wu [a], Xuecheng Wu [a,*], Jun Jin [b], Jian Guan [c]

[a] State Key Laboratory of Clean Energy Utilization, Zhejiang University, Hangzhou, 310027, Zhejiang, China
[b] Zhejiang Zheneng Jiahua Power Co., Ltd., Pinghu, 314201, Jiaxing, China
[c] Zhejiang Energy Group Co., Ltd., Hangzhou, 310027, Zhejiang, China

ARTICLE INFO

Keywords:
Wet flue gas desulfurization
Slurry droplets
Digital holography
In situ measurement
Coal-fired power unit

ABSTRACT

Wet flue gas desulfurization (WFGD) is a commonly utilized desulfurization technique. A major application of WFGD can be found in the coal-fired power plant, with up to 90% share of its market. Despite the fact that WFGD has been well developed and proven, its negative effects persist, e.g., entrainment pollution stemming from slurry droplet emission. In this study, we demonstrate *in situ* monitoring of flue gas slurry droplet emission in the coal-fired power unit using a self-made instrument based on digital holography, named the holographic slurry droplet monitor (HSDM), and gain insight into the key characteristics of slurry droplet emission through further statistics. HSDM exhibits superior accuracy in the respect of mass concentration, compared with conventionally accepted Mg^{2+} tracer method, and the maximum bias of the two is 5.61%. The application of HSDM in the real scenario of a 1000 MW coal-fired power unit is performed. After that, real-time slurry droplet measurement data is analyzed, revealing the key characteristics of slurry droplets, including size distribution and mass concentration, as well as factors associated with emission. Overall, high accuracy, real-time availability with a response time of 10 min, and multi-info acquisition in both size distribution and mass concentration make HSDM a remarkable alternative to the conventional method, enabling it to play a critical role in slurry droplet emission measurement.

1. Introduction

Wet flue gas desulfurization (WFGD) with the advantages of high desulfurization efficiency, well proven, and low operating cost, holds an important role among desulfurization technology. Thousands of boiler-involved industries deploy WFGD facilities in China. The SO_2 is removed by the absorption of limestone slurry and turns to sulphate that is further extracted and dewatered from the absorbent as gypsum. A major application of WFGD can be found in coal-fired power plant, with up to 90% share of its market, where the combustion of coal releases large amounts of sulfur oxides and the removal of SO_2 is an essential link of flue gas purification process. SO_2 emission is under strict control and its standards are well established over the world. The WFGD has been constantly improved in the past decades of engineering applications, giving the status quo that it is quite mature and reliable. Apart from the discussion of economic input and output, the impact of WFGD on particulate matter emission of flue gas is of great concern. In the WFGD process, as illustrated in Fig. 1, the upward flowing hot flue gas encounters the spraying downward slurry. Therefore, massive slurry droplets are released into flue gas and change the emission characteristics of particulate matter (PM). Extensive literature has reported on the influence of the WFGD on flue gas pollution emission, covering fine PM emission to ions emission, and so on. It has been found that the WFGD contributes to PM removal. Compared with the inlet flue gas of WFGD, over 50% PM was filtered when the flue gas was processed by WFGD, and the combination of WFGD and precipitator can achieve better removal efficiency up to 90% [1–3].

However, because of the entrainment of slurry droplets, the PM removal ability of WFGD is actually overestimated [1]. Slurry droplets entrainment has a distinct impact on PM emission characteristics. Unlike water vapor in flue gas, slurry droplets carry solid components and soluble salts. The weight percentage of solid components in slurry droplets is about 10% to 25% even higher, which mainly consists of limestone that comes from the WFGD process. Both solid components and soluble salts are released after liquid droplets evaporate or settle, leading to severe re-entrainment pollution. Though mist eliminator can remove slurry droplets, it is underperformance in removing slurry

* Corresponding author.
E-mail addresses: lzmfor@zju.edu.cn (Z. Lin), wuyingchun@zju.edu.cn (Y. Wu), wuxch@zju.edu.cn (X. Wu), jinjun2@zhenergy.com.cn (J. Jin), guanjian@zjenergy.com.cn (J. Guan).

https://doi.org/10.1016/j.fuel.2022.124813
Received 24 March 2022; Received in revised form 27 May 2022; Accepted 5 June 2022
Available online 22 June 2022
0016-2361/

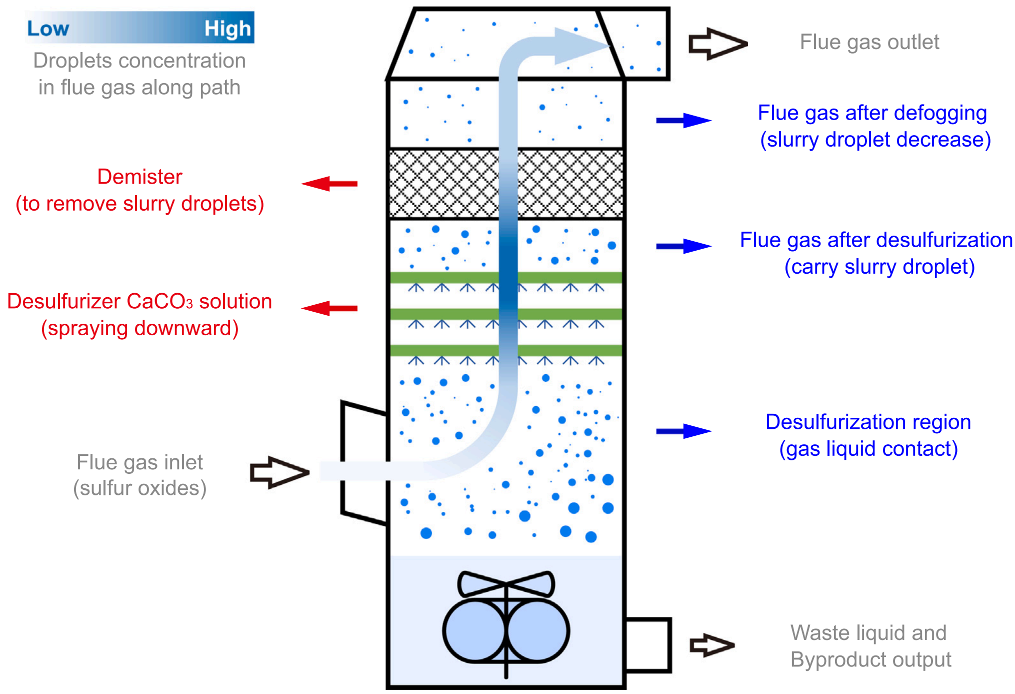

Fig. 1. Schematic of WFGD unit. The upward flowing hot flue gas encounters the spraying downward slurry, thereby carrying massive sensible slurry droplets.

droplets with a size less than 30 μm. And slurry droplets removal efficiency is under 20% ~ 30% when droplet size is below 15 μm[4,5]. As a consequence of that, the released gypsum crystal particle and fine unreacted limestone particle raise $PM_{2.5}$ and PM_{10} emission level [3,6]. The impact of WFGD on PM emission has been investigated by the experimental study on PM emission monitoring and PM component analysis [7–10], the numerical simulation on PM movement and collision [11,12]. Yet few studies focus on slurry droplets characterization and most of them are numerical simulations [5,13,14]. Nevertheless, investigations into slurry droplets in real scenarios from a quantitative perspective still lack enough attention and effort.

Slurry droplets in flue gas with the features of small size (0~30 μm), low number density (10~20 per cm^3) and impurities are difficult to be characterized by many advanced optical methods that based on light scattering concept. For the reason that most of the light scattering methods are in response to a single-point or flat ROI, which lacks productivity in the situation of low number density, e.g., phase Doppler anemometry (PDA) [15,16], interferometric particle imaging (IPI) [17–19]. Apart from that, the impurities inside slurry droplets change the refractive index and leave it an unknown parameter that is a key to inverse the real diameter of slurry droplets from the light scattering signal. The PDA has been used to measure slurry droplets in laboratory-level desulfurization setup [20,21], while the limitations of the PDA are obvious, e.g., single-point detection only, not suitable for droplets containing impurities. Flue gas sampling is regarded as the standard approach to obtaining slurry droplets in flue gas. Slurry droplet mass concentration can be calculated by Mg^{2+} tracer method [22,23]. However, the diameter and number density of slurry droplets are unavailable in sampling methods, whereas these two fundamental parameters are closely related to PM emission and also key to understanding the effectiveness of mist eliminators. As underlying technology for this study, digital holography may give a chance to overcome these deficiencies. In contrast to the light scattering methods, the holography can be conducted with the underpinning of the diffraction theory [24–26]. It cares less about the refractive index of target. More importantly, it is a three-dimension measurement method that has a large view of field and a depth of field, which makes it easy to cover more targets in one single shot. The typical applications of digital holography in spray measurement have achieved not only droplet size characterization, but contour, velocity, and spatial distribution analysis [27,28]. Similar applications can also be found in combustion diagnosis [29,30], microflow measurement [31,32], and so on, for both regular and irregular, homogeneous and non-homogeneous targets.

In this study, we demonstrate an *in situ* measurement of slurry droplets in flue gas by a self-made instrument based on digital holography, named holographic slurry droplet monitor (HSDM). Starting with the introduction of HSDM, the image resolution, algorithm workflow, and data statistics principles are presented. Then, the application of HSDM in the real scenario of a 1000 MW coal-fired power unit is performed. After that, real-time slurry droplet measurement data is analyzed, revealing the key characteristics of slurry droplets, including size distribution and mass concentration, as well as factors associated with emission.

2. Holographic slurry droplet monitor

2.1. Design

The HSDM adapts the in-line holography optical configuration so that the light source and recording device are placed on each side of the analysis zone, which is easy-to-use and robust, guaranteeing the stability of the HSDM in real situations. The HSDM consists of a recording arm, a light source arm, an extension arm, and a flange for fixation usage, as shown in Fig. 2. The recording arm and light source arm are connected by two stainless connectors, and the gap in the middle of the two connectors serves as the analysis zone for measurement, which has a width of 30 mm and a height of 60 mm. The extension arm and the flange in tail are used for mounting. In the in-line optical configuration, a continuous laser beam with a wavelength of 532 nm is first filtered by a pinhole spatial filter, then it is collimated into a columnar beam with a diameter of 12 mm. A telecentric lens and camera are fixed downstream of the laser path to record the holograms of slurry droplets. The camera resolution is 2448 × 2048, and the pixel size is 3.45 μm. The camera exposure time is set at 1 μs to suppress trail shadow induced by droplet movement. The telecentric lens has a

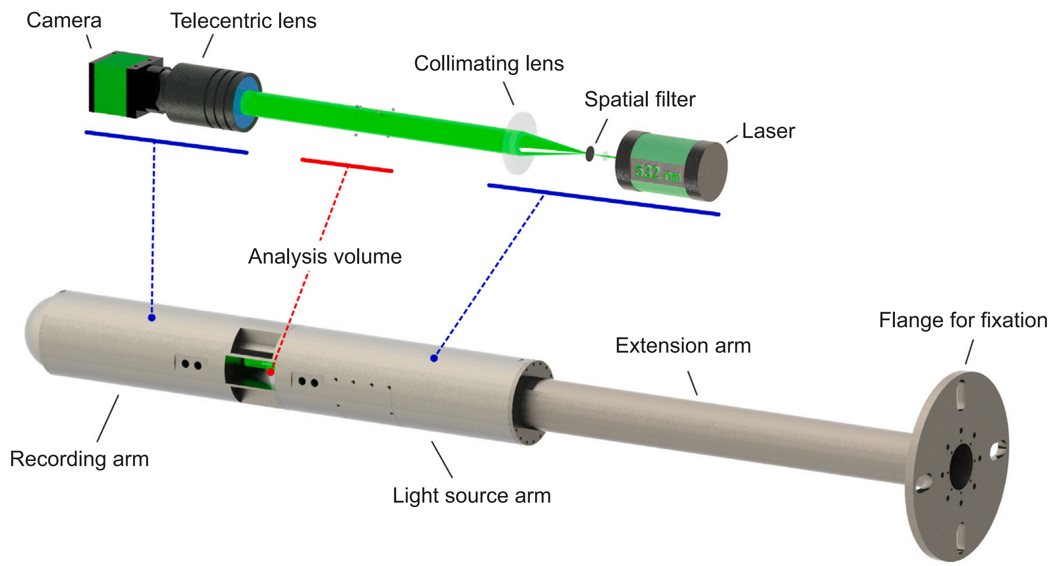

Fig. 2. Schematic of HSDM and in-line holography optical configuration inside. It consists of recording arm, light source arm, extension arm and a flange for fixation usage. The recording arm and light source arm carry recording device and light source, respectively, and the zone in the middle of the two serves as the measurement region.

Table 1
Key indicators of HSDM.

Item	Description
Effective measurement volume	$4.2 \times 3.5 \times 20$ mm^3
Effective droplet size range	$1.72 \sim 10^3$ μm
Effective concentration range	$0 \sim 10^4$ mg/Nm^3
Response time	less than 10 min
Housing temperature during operation	$0 \sim 60$ °C
Humidity during operation	$0 \sim 100\%$, relative

40 mm working distance and a magnification of 2×, thus the equivalent pixel size is 1.72 μm. Overall, the effective analysis zone volume of the HSDM can be up to $4.2 \times 3.5 \times 20$ mm^3 (see Table 1).

2.2. Resolution investigation

The resolution value represents the smallest distance between two objects that can be registered by an optical system, and it is often specified in line pairs per millimeter (lp/mm). The equivalent pixel value of the established optical system of HSDM is 1.72 μm. In other words, the resolution is up to 290 lp/mm in theory. But the real resolution is normally less than the value that the equivalent pixel defines. In this study, the resolution is specified through a 1951 USAF resolution test target. As illustrated in Fig. 3, the x-coordinate value refers to the distance from the focal plane to the investigated plane in the DOF direction. The maximum resolution value is available at the focal plane, which has a value of 203 lp/mm, meaning that the distinguishable smallest distance between two objects is 2.46 μm, and the resolution decreases with distance.

The analysis volume is defined as the product of the cross-section area and the length of DOF, and the cross-section area is already fixed according to the camera sensor size. The choice of DOF length decides the analysis volume. Thus, there is a trade-off between the analysis volume and the smallest object size. Since the weight of a slurry droplet is the cube of its diameter as well as its volume, the bigger slurry droplets make up the main part of the concentration. Therefore, it is reasonable to neglect small droplets. In this study, this is decided by slurry droplet size distribution feature, and the diameter threshold is considered to be 5 μm. Thus, the DOF value is set at 20 mm, in which the resolution is approximately 114 lp/mm, or alternatively, a distinguishable smallest distance of 4.38 μm.

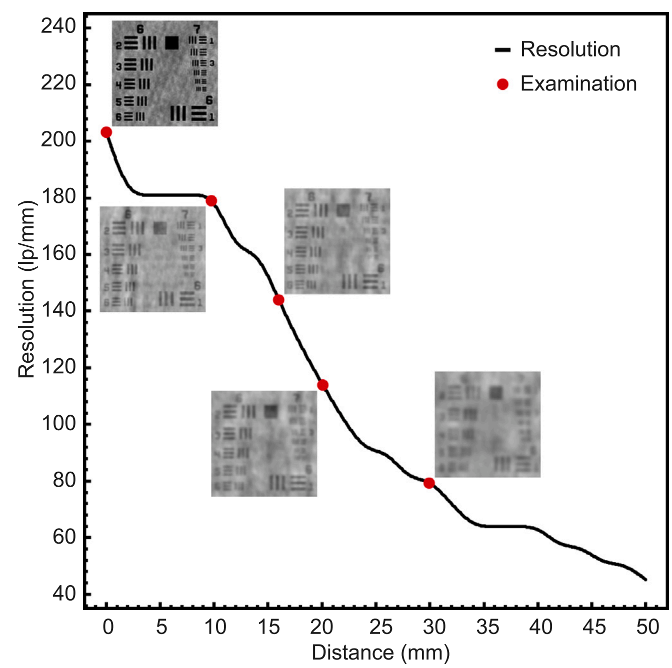

Fig. 3. Resolution of the optical configuration of HSDM at different DOF. Notice that the images after 0 mm are their holographic reconstruction results at the corresponding locations.

2.3. Algorithm workflow

Fig. 4 gives the algorithm workflow of the HSDM. The result at a given point in time is defined as the accumulation of a certain number of images results during that time period.

For the purpose of improving holographic processing speed, YOLOv5 [33], a fast and robust object detection machine learning algorithm, is adapted to pre-identify the hologram patterns of each image. Since the number density of slurry droplets is extremely low, it is frequently encountered that each image contains information from only a few or no droplets. Thus, handling of the whole image is unnecessary and time wasting. After pre-identification through the YOLOv5 algorithm, the valid regions that contain hologram patterns are intercepted out of the original image, and basically they are the holograms of a single droplet, followed by other processes. This treatment increases overall processing speed by a factor of 7 to 9. Another advantage of this treatment is that single-target hologram facilitates autofocusing process, allowing the use of simple and fast processing algorithm, in which the gray scale gradient variance methods [34] is adopted here. Hologram reconstruction procedure is based on the wavelet method, which can be found in the previous studies [35,36].

Assuming that N images are picked, each image is de-backgrounded and then followed with YOLOv5 object detection operation to get K valid regions.

Following that, the valid regions are subjected to regular holographic processing procedures, including reconstruction, autofocusing, and information extraction. The size distribution of slurry droplets can be quantified by the number share of slurry droplets in a different diameter zone. The mass concentration of slurry droplets is calculated using the formula

$$C = \frac{\left[\sum_1^N \sum_1^M \frac{4}{3}\pi\left(\frac{D_{N,M}}{2}\right)^3\right]\cdot\rho_w}{N\cdot M\cdot x\cdot y\cdot z}\cdot\frac{1}{\eta}\cdot\frac{1}{1-C_x}, \tag{1}$$

where the C is the slurry droplets concentration. The N is the number of images to be used for each calculation. The M is the total droplet number in the N^{th} image. The $D_{N,M}$ is the diameter of the M^{th} droplet in the N^{th} image. The ρ_w is the liquid density which is taken as 1000 kg/m^3 in the calculation. The x, y and z represent the width, height, and the length of the cutoff DOF of the ROI volume, respectively. The gas volume is adjusted to the volume under the condition of dry, 6% O_2 content, and standard temperature and pressure (STP), which is embodied in the correction factor η. The C_x is the percentage of solid content of slurry droplets.

2.4. Data validity analysis

The HSDM has a large measurement volume, yet it can only cover a few droplets in one single shot, for the reason that the number density of slurry droplets in flue gas is quite low, as mentioned above. The result of a point of time is based on the analysis result of the slurry droplets holographic images that are captured around the point of time. Lack of enough slurry droplet samples will inevitably leads to random results. Thus, the accumulation of multiple-image results will be necessary to acquire sufficient samples and eliminate the randomness of analysis. Meanwhile, it should be paid attention that excessive analysis will add time cost which is bad for real-time performance. To this end, a straightforward way is to investigate the variations in accumulative average values when the number of involved images increases, including the variations of size distribution and average concentration. The following study was carried out to specify the number of images used in each round.

For the size distribution feature, as illustrated in Fig. 5(a), there are eight diameter zones, with an interval of 5 μm, and each bar consists of the slurry droplets number shares at each diameter zone. Thus, the sum of the eight zones' share is 100%. In this study, the number of images gradually increases from 20 to 220 with an interval of 10. As revealed in Fig. 5(a), when there are enough images involved in the calculation, the number shares of each diameter zone tend to be invariable, in which the number of images is estimated to be larger than 140. Likewise, for the same case, Fig. 5(b) shows the mass concentration variation. It remains largely unchanged when the number of images exceeds 140, which can be told by the relative deviation of mass concentration.

A close examination was conducted on 25 cases with their relative deviation, the average relative deviation, and the standard deviation (SD) of relative deviation analyzed, as shown in Fig. 6. There are 25 sets of data for each situation that correspond to a certain number of images. The sampling distribution of the relative deviation value of the 25 cases is symmetrical, and the averages of their relative deviations are

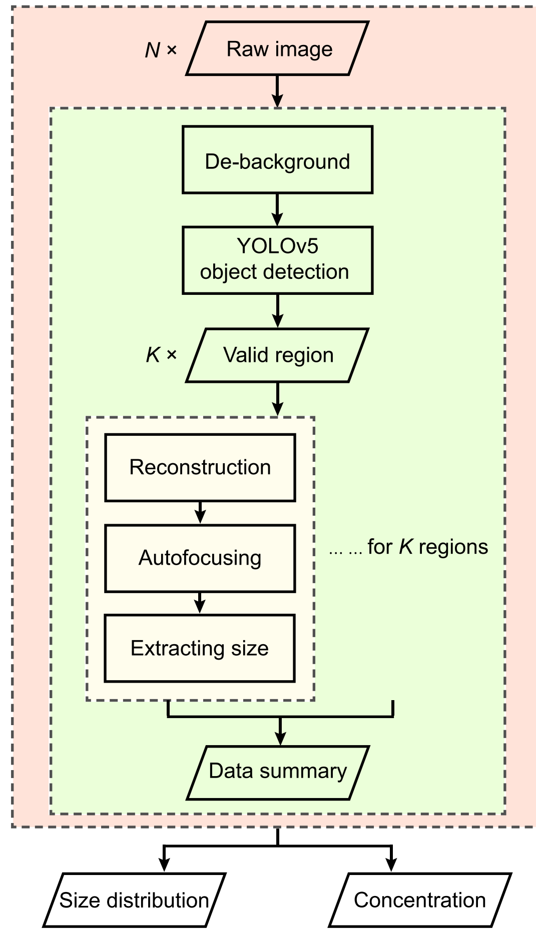

Fig. 4. Algorithm workflow of HSDM. Assuming that N images are picked out, each image is first de-backgrounded, then followed with the YOLOv5 object detection operation to get K valid regions. After that, the valid regions are then subjected to regular holographic processing procedures.

approximately equal to 0 for all situations, which indicates the samples are well represented with negligible sampling error. In Fig. 6(a), the diameter zone of 10 to 15 μm is listed out for analysis on the grounds that this zone basically reflects the overall evolution trend of the size distribution. The relative deviation is defined as the relative value change between the former and later situation. With the number of images exceeding 120, the relative deviations are mostly distributed in the narrow region of −5% to 5%, and the SD of relative deviation is also less than 5%. These fact gives a conclusion that the analysis on 120 images could yield a reasonable result on size distribution. Similarly, the mass concentration feature of the same 25 cases is being investigated. As illustrated in Fig. 6(b), the SD of relative deviation decreases from 5% downwards at the point when the number of images is equal to 140. Thus, 140 images will be sufficient to provide a stable statistical figure on mass concentration with acceptable randomness in most of the cases.

From the above two aspects, the accumulation of results from 140 images can serve as a reasonable result in terms of the size distribution and mass concentration. Adding more images will result in a value variation of 4% and 5% for the size distribution and mass concentration, respectively, and these levels of variation are well acceptable.

3. Accuracy validation

The accuracy validation of HSDM is conducted in the field testing of a 1000 MW coal-fired power unit, by comparing slurry droplets

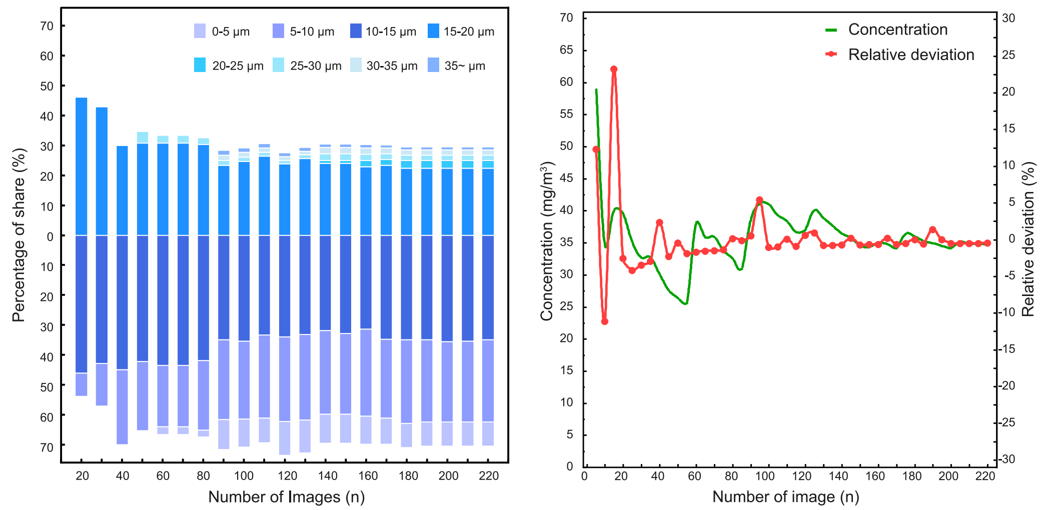

(a) (b)

Fig. 5. Result of a certain point in time. (a) The variation in size distribution when the number of joined images increases. Eight diameter zones are divided, with an interval of 5 μm. Each bar represents the size distribution that consists of the number share percentage of each diameter zone. (b) The variation in concentration when the number of images increases. The relative deviation is the value variation between the former and the latter.

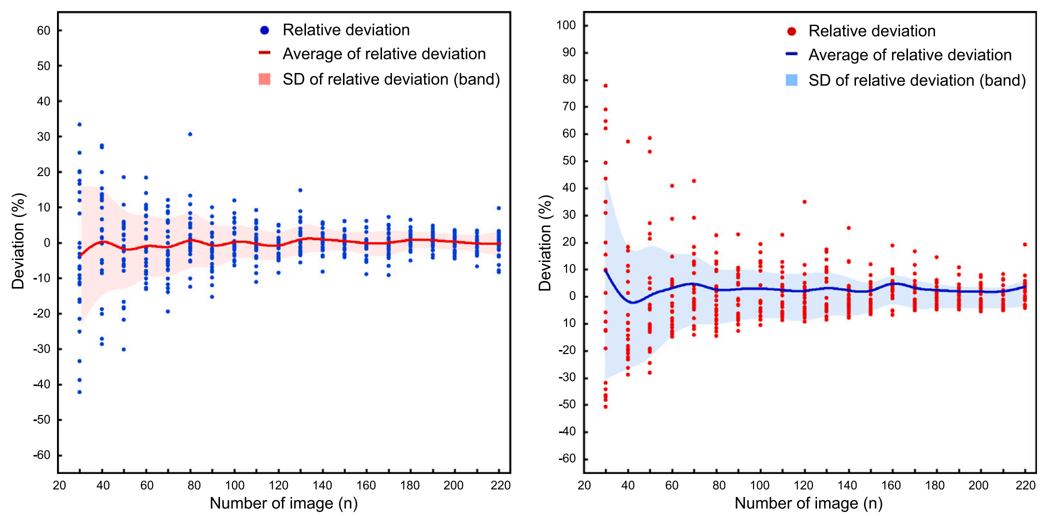

(a) (b)

Fig. 6. Results of 25 cases. (a) The relative deviation, average of relative deviation, and the SD of relative deviation of the size zone of 10 to 15 μm, when the number of images increases. (b) The relative deviation, average of relative deviation, and the SD of relative deviation of concentration, when the number of images increases.

Table 2
Comparison of slurry droplets concentration measurement result by Mg^{2+} tracer method and HSDM.

No.	$C_{Mg,0}$ (mg/L)	C_x (%)	η	V_g (Nm^3)	$C_{Mg,s}$ (mg/L)	C_1 (mg/Nm^3)	C_2 (mg/Nm^3)	Bias (%)
1	1253.788	26.01	0.841	0.673	0.396	31.709	33.487	5.61
2	1253.788	26.01	0.841	0.673	0.321	25.666	26.533	3.38
3	1314.138	19.36	0.775	0.673	0.439	27.337	28.402	3.90
4	1314.138	19.36	0.775	0.775	0.416	25.817	24.562	−4.86

concentration obtained by the HSDM and the Mg^{2+} tracer method in the same time period. The test location was picked at the outlet of the WFGD tower. The Mg^{2+} tracer method consists of two steps that are flue gas sampling and Mg^{2+} concentration analysis. For the first step, a mist droplet trap is utilized to sample slurry droplets. Fig. 7 gives the schematic of the flue gas sampling operation. In addition to slurry droplets, the condensate water will also be collected inevitably during the sampling step. Therefore, a calibration step is necessary to infer the real slurry droplet content. The most acceptable criteria is based on Mg^{2+} for the reason that the Mg^{2+} concentration is relative stable within the WFGD. The slurry droplets and WFGD slurry have same Mg^{2+} concentration, thus this factor can be used to exclude the content of condensate water. Eq. (2) gives the slurry droplet mass concentration calculation formula.

$$C = \frac{C_{Mg,s} \cdot V_{s,l} \cdot 10^3}{C_{Mg,0} \cdot V_{s,g} \cdot \eta \cdot (1 - C_x)}. \tag{2}$$

The C is the slurry droplet mass concentration. The $C_{Mg,s}$ is the Mg^{2+} concentration of the liquid sample. The $V_{s,l}$ is the analytical volume of the liquid sample, including slurry droplets and condensate water. The

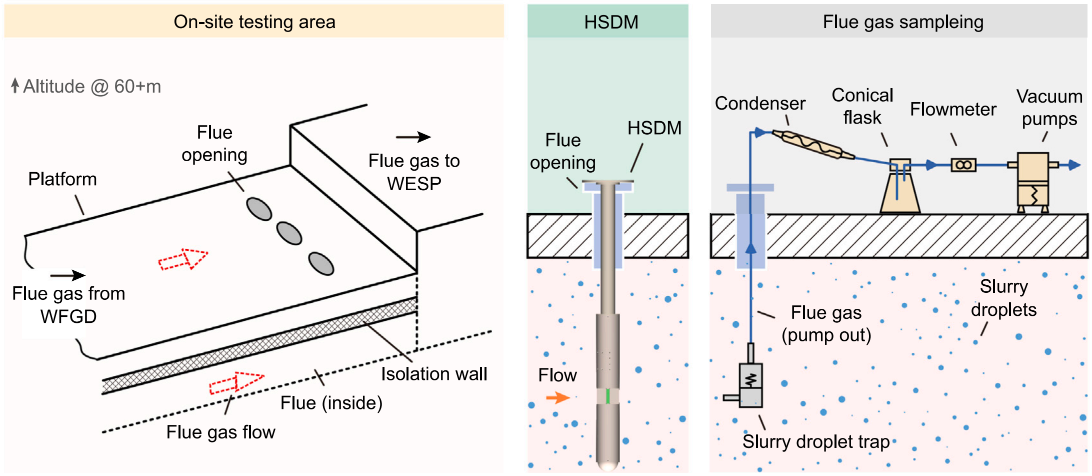

Fig. 7. Schematic of on-site testing area, the installation of HSDM on flue, and the flue gas sampling operation to collect slurry droplets for Mg^{2+} tracer analysis. WEPS: Wet electrostatic precipitator.

$V_{s,g}$ is the sampled flue gas volume, and it was adjusted to the volume under the condition of dry, 6% O_2 content, and standard temperature and pressure (STP), which is embodied in the correction factor η. The $C_{Mg,0}$ is the Mg^{2+} concentration of WFGD slurry. The C_x is the percentage of solid content in the WFGD slurry. Liquid density is taken as 1000 kg/m^3 in the calculation.

In the validation work, flue gas was pumped out of flue, with a sampling flow rate of 20 L/min and a collecting time of 40 min for each round. The slurry droplets were first captured by the slurry droplet trap. Then the flue gas flowed through the condensation bottle, allowing the second collection of leaking slurry droplet particularly the small size droplets. The total slurry droplet content was the sum of the two, and they were flushed together for Mg^{2+} concentration analysis purpose. The WFGD slurry was collected separately which were directly sampled from the WFGD tower. The high performance liquid chromatography (HPLC, Agilent Infinity 1260 II) and inductively coupled plasma mass spectrometry (ICP-MS, Agilent Technologies 7800 ICP-MS) were applied to analyze the Mg^{2+} concentration of the slurry droplets sample and WFGD slurry. Four comparisons were performed for accuracy validation here, as illustrated in Table 2. The C_1 and C_2 refers to the measurement results of Mg^{2+} tracer methods and HSDM, respectively. The biases of the two vary from −4.86% to 5.61%. Compared with the widely accepted 10% bias in industrial situations, this level of bias confirms the reliability of HSDM.

4. Slurry droplet features

4.1. Slurry droplet hologram

Fig. 8 shows a typical hologram recorded by HSDM, which has been de-backgrounded. As can be seen, the slurry droplet hologram is easily identifiable without too much interference, which benefits from the robust in-line optical configuration and solid structural design. After pre-identification, reconstruction, and autofocusing operation, the two-dimensional contours of the slurry droplets can be restored from the hologram. There are 5 slurry droplets with a diameter of 12 μm to 16 μm. The number density of slurry droplets in flue gas is extremely low. Despite the large measurement volume of HSDM, it can only capture 3 to 10 droplets in a single shot on average. It is obvious that their holographic patterns account for a very small area of the whole image. Therefore, the pre-identification operation by the YOLOv5 object detection algorithm is very helpful to get rid of data redundancy and improve processing speed. In addition to that, it allows the separate processing of each target that has a different image grayscale level, which will facilitate the size extraction process. The five slurry droplets

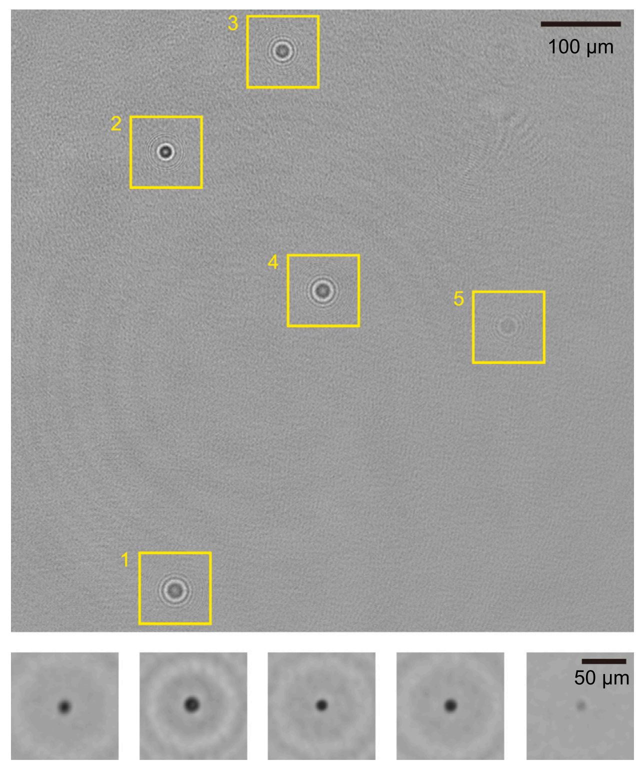

Fig. 8. Typical hologram recorded by HSDM, and reconstruction results of the five marked areas that correspond to five slurry droplets.

in Fig. 8 have different degrees of clarity that essentially because their image grayscale values are not the same. Therefore, different grayscale thresholds will be used to extract targets.

4.2. Slurry droplet size distribution

The size distribution of slurry droplets plays a fundamental role in PM emission for the reason that different droplet sizes result in different levels of sedimentation and other physicochemical reactions.

An overview of statistics data obtained under different flue gas conditions and system operating conditions is performed here, as illustrated in Fig. 9. As can be seen, the size distribution has single-peaked characteristic, and the peak falls in the range of 5 μm to 10 μm. Most of

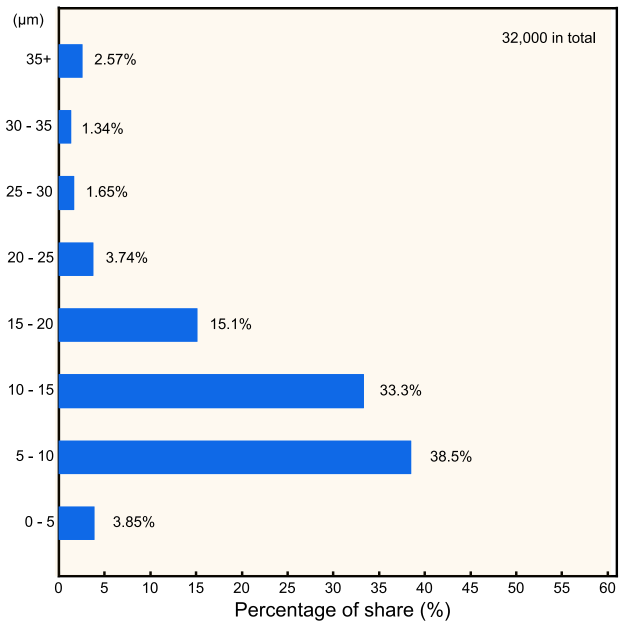

Fig. 9. Slurry droplets size distribution. A total of 32,000 slurry droplets are included here.

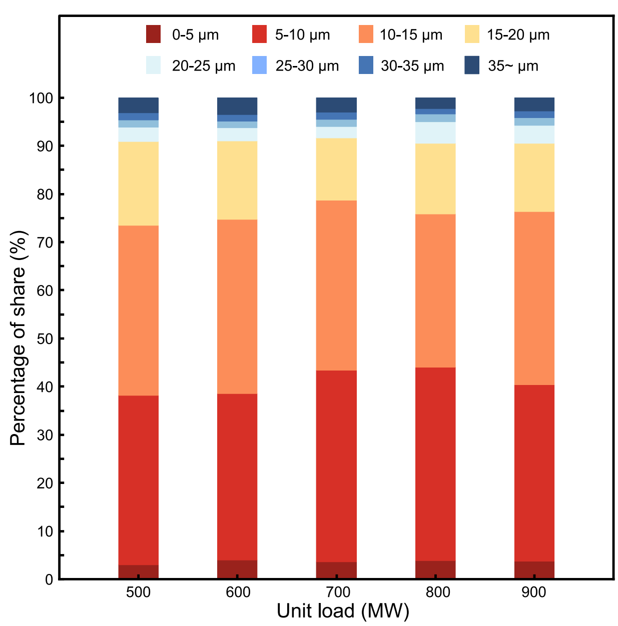

Fig. 10. Slurry droplets size distribution at different load.

the slurry droplets have a diameter of 5 μm to 15 μm, which accounts for 60 to 75% of the total. In addition, the slurry droplets with diameters of over 30 μm amount to as little as 5% of the share. Generally, the size distribution feature clearly reflects the removal performance of the eliminator for slurry droplets in flue gas, and it is consistent with the existing investigations into eliminator. The eliminator has an effective removal ability for slurry droplets over 30 μm, yet it underperforms for those below 20 μm. It should be mentioned that the number share of the diameter range of 0 μm to 5 μm is actually unrepresentative due to the fact that the HSDM limited by its effective resolution is poor at this level of metric. Moreover, there is no significant change in size distribution when the unit load changes, as shown in Fig. 10.

4.3. Slurry droplet concentration

Slurry droplet emission is basically quantified by its mass concentration according to official regulation, and the established emission standard in China is 75 mg/m^3. As shown in Fig. 11, the real-time slurry droplet mass concentration from 7-day monitoring data, as well as flue gas velocity and SO_2 emission in the same time period, is disclosed here. The 10-minute curve of slurry droplet mass concentration is directly acquired from HSDM, which is set to deliver data every 10 min, while the 60-minute curve comes from the average of that hour. Flue gas velocity is calculated through total flue gas volume and the cross-sectional area of the absorber tower. It should be noted that the operation conditions of the WFGD system keep largely unchanged during this time period. There are two recycle pumps running with constant output power, meaning that the absorber slurry supply remains unchanged. Although the operating differential pressure between the inlet and outlet of the eliminator is affected by the unit load, it remains largely stable at 30 to 150 Pa and the eliminator is performing well.

The slurry droplet mass concentration of the current 1000 MW coal-fired unit swings between 5 and 60 mg/m^3 and exceeds 75 mg/m^3 only in rare cases, meeting the Chinese national emission standards. In terms of general trends, the slurry mass concentration varies up and down with the flue gas velocity, especially at the point when the latter changes dramatically, as illustrated in Fig. 11. Concretely, it is considered as a result of the fact that absorber slurry inside WFGD is atomized into small droplets and maintained in adequate condition. Droplets of sizes ranging from 0 to 30 μm have good features of following flue gas. In the presence of ample atomized slurry droplets, the higher the flue gas velocity, the better the ability of flue gas to entrain slurry droplets. For the current 1000 MW coal-fired unit, at the flue gas velocity of 1 m/s to 3.5 m/s, the effect of the flue gas entrainment outweighs the effect of flue gas dilution capacity. Therefore, there is a positive correlation between slurry mass concentration and flue gas velocity.

In addition, the volume of flushing water used during the mist eliminator cleaning operation is recorded. The data given in Fig. 11 shows that it has negligible effect on slurry droplet emission due to the flushing water volume being significantly smaller than the absorber slurry release during WFGD operation.

With a removal effect of up to 99.5%, SO_2 emission has been maintained at a pretty low level, and its variations may fail to reflect any correlations related to slurry droplet emission. However, at the moment when the flue gas velocity changes dramatically, it still follows the trend, with SO_2 emission showing a positive correlation with the flue gas velocity, as shown in Fig. 11. In fact, SO_2 removal effect benefits from low flue gas velocity, which creates a long residual time for the desulfurization reaction inside WFGD. Since slurry droplet emission are measured at the outlet of the WFGD, there is less connection between SO_2 emission and slurry droplet emission.

5. Conclusion

The purpose of this study is to demonstrate a self-made instrument, named the holographic slurry droplet monitor (HSDM), that can be used to *in situ* measure the size distribution and mass concentration of slurry droplets in flue gas. Following that, the data analysis of HSDM in a real scenario of a 1000 MW coal-fired power unit is performed.

HSDM uses an in-line holography optical configuration with a large measurement volume of 4.2 × 3.5 × 20 mm^3. Meanwhile, the data processing procedures adopting machine learning algorithm greatly eliminates data redundancy and enhances overall processing speed by a factor of 7 to 9, enabling it to deliver result at a point in time within 10 min and ensuring its fast analysis capability even with large measurement volume. In the comparison with traditionally accepted Mg^{2+} tracer method, HSDM shows high accuracy in the respect of mass concentration, and the maximal bias of the two is 5.61%.

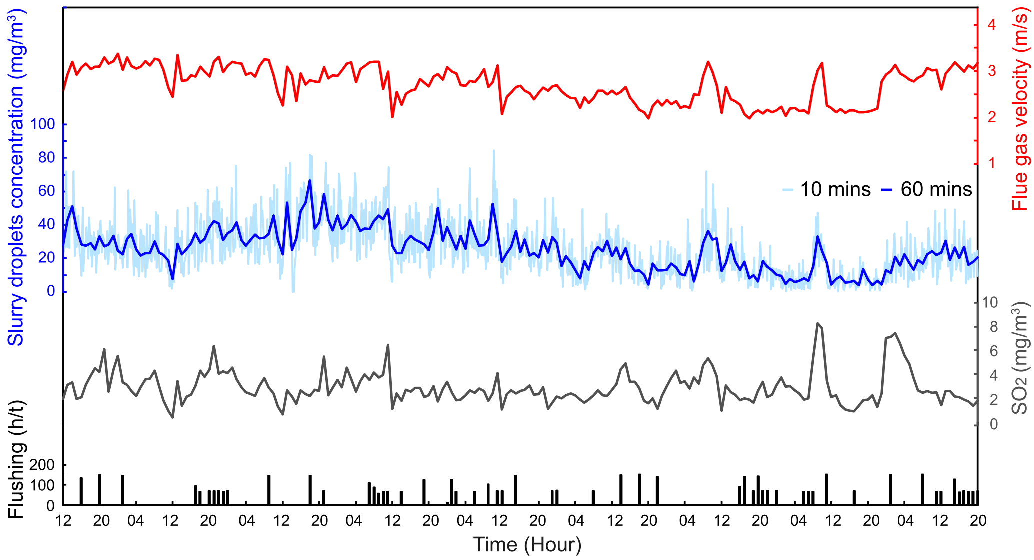

Fig. 11. 7 days of real-time hourly slurry droplets mass concentration, flue gas velocity, and SO_2 emission monitoring data. The concentration has been adjusted to the condition of dry, 6% O_2 content, and STP. Flushing refers to the mist eliminator flushing water volume in ton per hour.

The application of HSDM in the real scenario of a 1000 MW coal-fired power unit is performed, revealing the key characteristics of slurry droplets, including size distribution and mass concentration. The size distribution of slurry droplets is found to be unimodal, with over 70% falling in the diameter range of 5 μm to 15 μm. According to 7-day real-time slurry droplet emission monitoring data, the slurry droplet mass concentration swings between 5 and 60 mg/m^3, fulfilling Chinese national emission requirements. There is a distinct positive correlation between slurry droplet mass concentration and flue gas velocity. a higher flue gas velocity will increase slurry droplet emission at a flue gas velocity in the range of 1 m/s to 3.5 m/s.

Overall, high accuracy, real-time availability with a response time of 10 min, and multi-info acquisition in both size distribution and mass concentration make HSDM a remarkable alternative to the traditional method for the effective detection and quantitative investigation of slurry droplet emission.

CRediT authorship contribution statement

Zhiming Lin: Writing – original draft, Investigation, Software, Data curation. **Yingchun Wu:** Writing – review & editing, Visualization. **Xuecheng Wu:** Conceptualization, Methodology, Validation. **Jun Jin:** Resources, Investigation. **Jian Guan:** Validation.

Declaration of competing interest

The authors declare that they have no known competing financial interests or personal relationships that could have appeared to influence the work reported in this paper.

Funding

Project supported by the Science and Technology Project of Zhejiang Energy Group Co., Ltd., No. ZNKJ-2019-016.

References

[1] Álvarez-Ayuso E, Querol X, Tomás A. Environmental impact of a coal combustion-desulphurisation plant: Abatement capacity of desulphurisation process and environmental characterisation of combustion by-products. Chemosphere 2006;65(11):2009–17.
[2] Córdoba P. Status of flue gas desulphurisation (FGD) systems from coal-fired power plants: Overview of the physic-chemical control processes of wet limestone FGDs. Fuel 2015;144:274–86.
[3] Pan D, Wu H, Yang L. Fine particle transformation during the limestone gypsum desulfurization process. Energy Fuels 2016;30(11):9737–44.
[4] Zamora B, Kaiser A. Comparative efficiency evaluations of four types of cooling tower drift eliminator, by numerical investigation. Chem Eng Sci 2011;66(6):1232–45.
[5] Guan L, Yuan Z, Yang L, Gu Z. Numerical study on the penetration of droplets in a zigzag demister. Environ Eng Sci 2016;33(1):35–43.
[6] Wang A, Song Q, Tu G, Wang H, Yue Y, Yao Q. Influence of flue gas cleaning system on characteristics of PM 2.5 emission from coal-fired power plants. Int J Coal Sci Technol 2014;1(1):4–12.
[7] Meij R, Te Winkel B. The emissions and environmental impact of PM10 and trace elements from a modern coal-fired power plant equipped with ESP and wet FGD. Fuel Process Technol 2004;85(6–7):641–56.
[8] Álvarez-Ayuso E, Querol X, Tomás A. Environmental impact of a coal combustion-desulphurisation plant: Abatement capacity of desulphurisation process and environmental characterisation of combustion by-products. Chemosphere 2006;65(11):2009–17.
[9] Wang H, Song Q, Yao Q, Chen C-h. Experimental study on removal effect of wet flue gas desulfurization system on fine particles from a coal-fired power plant. Proc-Chin Soc Electr Eng 2008;28(5):1.
[10] Chen Z, You C, Liu H, Wang H. The synergetic particles collection in three different wet flue gas desulfurization towers: a pilot-scale experimental investigation. Fuel Process Technol 2018;179:344–50.
[11] Wang A, Song Q, Ji B, Yao Q. Effect of droplet deformation on inertial and thermophoretic capture of particles. Atmos Environ 2016;127:187–95.
[12] Huang Y, Zheng C, Li Q, Zhang J, Guo Y, Zhang Y, Gao X. Numerical simulation of the simultaneous removal of particulate matter in a wet flue gas desulfurization system. Environ Sci Pollut Res 2020;27(2):1598–607.
[13] Estakhrsar MH, Rafee R. Effects of wavelength and number of bends on the performance of zigzag demisters with drainage channels. Appl Math Model 2016;40(2):685–99.
[14] Yang L, Xu M, Wang J, Song L, Wang J. Experimental and numerical analysis of a demister with vortex generators. Chin J Chem Eng 2021;33:83–95.
[15] Tropea C. Optical particle characterization in flows. Annu Rev Fluid Mech 2011;43:399–426.
[16] Albrecht H-E, Damaschke N, Borys M, Tropea C. Laser Doppler and phase Doppler measurement techniques. Springer Science & Business Media; 2013.
[17] Glover A, Skippon S, Boyle R. Interferometric laser imaging for droplet sizing: a method for droplet-size measurement in sparse spray systems. Appl Opt 1995;34(36):8409–21.
[18] Kawaguchi T, Akasaka Y, Maeda M. Size measurements of droplets and bubbles by advanced interferometric laser imaging technique. Meas Sci Technol 2002;13(3):308.
[19] Dehaeck S, Van Beeck J. Designing a maximum precision interferometric particle imaging set-up. Exp Fluids 2007;42(5):767–81.
[20] Cui L, Zhang L, Li B, Dong Y, Yuan X, Ma C. Effect investigation of composite humidification way on wall deposition of water droplets and desulfurization process in semi-dry CFB-FGD tower. In: 2010 Asia-pacific power and energy engineering conference. IEEE; 2010, p. 1–5.

[21] Pan D, Wu H, Yang L. Investigation of the relationship between droplet and fine particle emissions during the Limestone–Gypsum wet flue gas desulfurization process. Energy Fuels 2017;31(6):6472–7.

[22] Standards CN. Test method for chemical and physical properties of limestone-gypsum wet flue gas desulfurization system. Standardization Administration of China; 2015, DL/T1483-2015.

[23] Wu X-C, Zhao H-F, Zhang Y-X, Zheng C-H, Gao X. Measurement of slurry droplets in coal-fired flue gas after WFGD. Environ Geochem Health 2015;37(5):915–29.

[24] Murata S, Yasuda N. Potential of digital holography in particle measurement. Opt Laser Technol 2000;32(7–8):567–74.

[25] Javidi B, Tajahuerce E. Three-dimensional object recognition by use of digital holography. Opt Lett 2000;25(9):610–2.

[26] Guildenbecher DR, Gao J, Reu PL, Chen J. Digital holography simulations and experiments to quantify the accuracy of 3D particle location and 2D sizing using a proposed hybrid method. Appl Opt 2013;52(16):3790–801.

[27] Lü Q, Chen Y, Yuan R, Ge B, Gao Y, Zhang Y. Trajectory and velocity measurement of a particle in spray by digital holography. Appl Opt 2009;48(36):7000–7.

[28] Yang Y, Kang B-s. Digital particle holographic system for measurements of spray field characteristics. Opt Lasers Eng 2011;49(11):1254–63.

[29] Wu Y, Wu X, Yao L, Xue Z, Wu C, Zhou H, Cen K. Simultaneous particle size and 3D position measurements of pulverized coal flame with digital inline holography. Fuel 2017;195:12–22.

[30] Yao L, Yu L, Lin X, Wu Y, Chen J, Zheng C, Wu X, Gao X. High-speed digital off-axis holography to study atomization and evaporation of burning droplets. Combust Flame 2021;230:111443.

[31] Kim M-K. Applications of digital holography in biomedical microscopy. J Opt Soc Korea 2010;14(2):77–89.

[32] Merola F, Miccio L, Memmolo P, Paturzo M, Grilli S, Ferraro P. Simultaneous optical manipulation, 3-D tracking, and imaging of micro-objects by digital holography in microfluidics. IEEE Photonics J 2012;4(2):451–4.

[33] Jocher G. ultralytics/yolov5. Zenodo; 2020, http://dx.doi.org/10.5281/zenodo.4154370, https://github.com/ultralytics/yolov5.

[34] Pech-Pacheco JL, Cristóbal G, Chamorro-Martinez J, Fernández-Valdivia J. Diatom autofocusing in brightfield microscopy: a comparative study. In: Proceedings 15th international conference on pattern recognition, Vol. 3. IEEE; 2000, p. 314–7.

[35] Malek M, Coëtmellec S, Allano D, Lebrun D. Formulation of in-line holography process by a linear shift invariant system: application to the measurement of fiber diameter. Opt Commun 2003;223(4–6):263–71.

[36] Yingchun W, Xuecheng W, Jing Y, Zhihua W, Xiang G, Binwu Z, Linghong C, Kunzan Q, Gréhan G, Kefa C. Wavelet-based depth-of-field extension, accurate autofocusing, and particle pairing for digital inline particle holography. Appl Opt 2014;53(4):556–64.